

***In-situ* NEXAFS Analysis of the Mg-Pd nanoparticles during the hydro-/dehydrogenation**

Satoshi Ogawa¹, Taishi Fujimoto², Tsuyoshi Mizutani², Masahiro Ogawa³, Chihiro Yogi³, Toshiaki Ohta³, Tomoko Yoshida^{2, 4}, Shinya Yagi^{2, 4}

1) *Department of Quantum Engineering, Graduate School of Engineering, Nagoya University, Furo-cho, Chikusa-ku, Nagoya, 464-8603, Japan*

2) *Department of Materials, Physics and Energy Engineering, Graduate School of Engineering, Nagoya University, Furo-cho, Chikusa-ku, Nagoya, 464-8603, Japan*

3) *The SR center, Ritsumeikan University, 1-1-1 Noji-Higashi, Kusatsu, Shiga, 525-8577, Japan*

4) *EcoTopia Science Institute, Nagoya University, Furo-cho, Chikusa-ku, Nagoya, 464-8603, Japan*

Abstract

The change of the chemical state of the Mg-Pd nanoparticles (Mg-Pd NPs) during hydro-/dehydrogenation has been investigated by the NEXAFS measurements under the *in-situ* condition. The Mg-Pd NPs have been fabricated by the gas evaporation method using He gas and embedded in the fluorine resin in order to protect the Mg-Pd NPs from the oxidation of the Mg-Pd NPs. Pd L₃-edge NEXAFS measurements have been carried out under the flowing the diluted hydrogen gas (4 wt% H₂) and pure He gas for the hydrogenation and dehydrogenation of the Mg-Pd NPs, respectively. The *in-situ* Pd L₃-edge NEXAFS analyses have revealed that the Pd phases in the Mg-Pd NPs are hydrogenated under the diluted hydrogen gas atmosphere. The subsequent dehydrogenation of the Pd phases has not been observed under the He gas. This result indicates that the dehydrogenation reaction of the Pd has been inhibited by the irreversible migration of the Mg toward the surface of the Mg-Pd NPs.

1. Introduction

Hydrogen storage material is the essential component in the sustainable hydrogen energy system. The role of the hydrogen storage material in the system is the storage tank of hydrogen which is the energy carrier between the electric energy supply and the energy consumer. The properties required for the hydrogen storage material are high storage capacity and energetic efficiency i.e. the storage and release of the hydrogen under the low temperature and low pressure of hydrogen gas. Magnesium (Mg) is the most promising material for the application of hydrogen storage because of high storage capacity up to 7.6 wt% as a result of the hydrogenation of Mg. The problems of Mg for the practical use are the high temperature more than 350 °C and high pressure of the hydrogen gas more than 3 MP during the hydro-/dehydrogenation reactions of Mg. These problems are caused by the low surface activity of Mg and the difficulty of the diffusion of hydrogen atoms through the Mg hydride (MgH₂) [1].

The NPs composed of Mg and palladium (Mg-Pd NPs) are expected to overcome the problems for the practical use of the Mg as the hydrogen storage materials. The surface activity of Mg is improved by the deposition of transition metal atom on the surface of Mg. The Mg thin film capped by Pd can uptake and release the hydrogen gas of 0.1 MPa under the room temperature because of the high hydrogen dissociation activity of Pd [2]. However, the diffusion length of hydrogen inside of the Mg bulk is limited by MgH₂ layer [1]. The scale-down of the size of Mg to nano-meter order is favorable for the further improvement of hydrogen diffusion kinetics.

In our previous work, the Mg-Pd NPs have fabricated by the gas evaporation method using helium (He) gas [3]. The sizes of the Mg-Pd NPs have distributed in the narrow range of 2-10 nm. The hydrogen storage capacity of the Mg-Pd NPs has been investigated by means of quartz crystal microbalance (QCM) technique [4, 5]. Fig. 1 shows the pressure-composition (P-C) isotherms for hydro/dehydrogenation of the Mg-Pd NPs. The 1st plateau at ~0.3 Torr and the second one at ~60 Torr have been attributed to the hydrogen storage of Mg and Pd phases, respectively [6, 7]. Although Mg-Pd NPs have been able to storage hydrogen up to 4.6 wt% at the 1st hydrogenation, the release of hydrogen and 2nd hydrogen storage have not been observed in Fig. 1. It is considered that the change of the chemical state of the Mg-Pd NPs has caused the degradation of the hydrogen storage capacity.

In this study, we have investigated the chemical state of the Mg-Pd NPs by the near Pd L₃-edge X-ray absorption fine structure analysis (Pd L₃-edge NEXAFS). The NEXAFS measurements have been carried out under the *in-situ* condition. *In-situ* NEXAFS provides direct information on the change of the chemical state of the Mg-Pd NPs during the

hydro-/dehydrogenation. Furthermore, the surface chemical state of the Mg-Pd NPs has been investigated by the X-ray photoelectron spectroscopy (XPS) method without the exposure of the Mg-Pd NPs to the air.

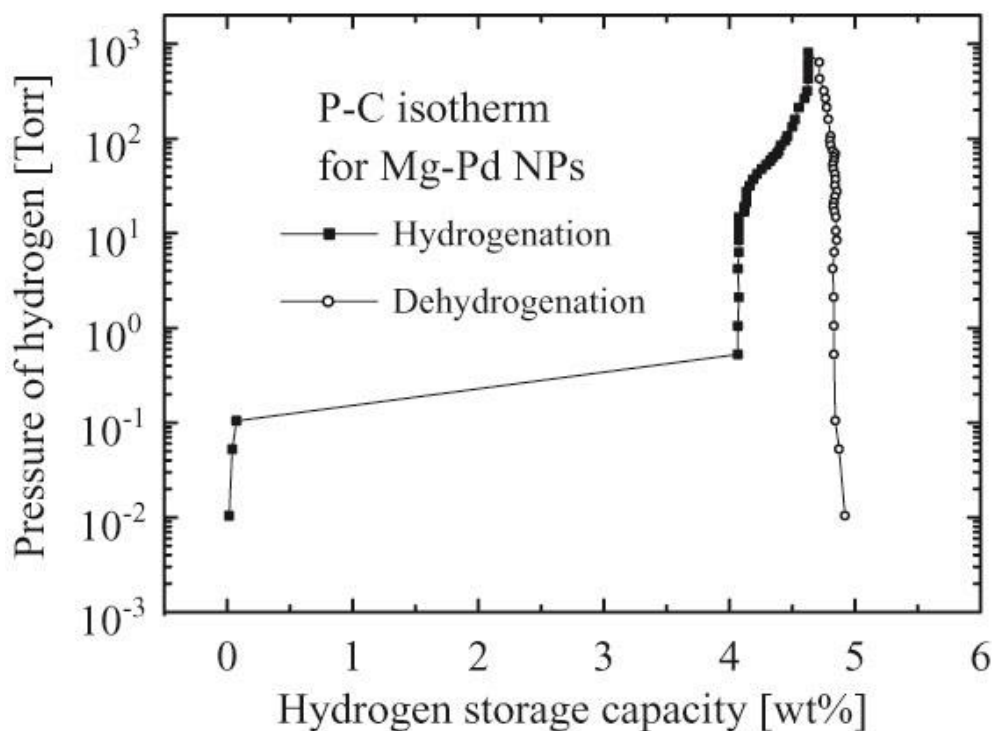


Fig. 1 The P-C isotherms for the hydro-/dehydrogenation of the Mg-Pd NPs at 303 K.

2. Experimental

Fabrication of the Mg-Pd nanoparticles

The Mg-Pd NPs were fabricated by the gas evaporation method using He gas (purity: 99.99995 %) [3]. The gas evaporation method is suitable for the fabrication of NPs with clean surfaces i.e. absence of surfactants and contaminations. The rod shaped Mg and Pd wire were used as the evaporation sources. These sources were equipped in the same evaporation chamber and were evaporated simultaneously under 60 Torr of He gas. The Mg-Pd NPs have been formed by the aggregation of the evaporated Mg and Pd atoms under the He gas atmosphere. The Mg-Pd NPs were deposited on the Ni polycrystalline substrate and the polypropylene (PP) film (2.8 μm^2). Fig. 2 shows the bright field image of the Mg-Pd NPs obtained by the transmission electron microscopy (TEM). The average diameter of Mg-Pd NPs was evaluated to be 5.9 nm. TEM bright field image in Fig.2 reveals that Mg-Pd NPs have been covered with oxide layer due to the air oxidation of Mg [8].

XPS measurement

After the fabrication of the Mg-Pd NPs, the fabrication chamber of the NPs was evacuated to high vacuum of $\sim 1 \times 10^{-7}$ Torr. The Mg-Pd NPs deposited on the Ni substrate were transferred to the ultra-high vacuum chamber ($\sim 5 \times 10^{-10}$ Torr) for the XPS measurement. The XPS measurements were performed using Mg K α X-ray (1253.6 eV) source and a hemispherical electron energy analyzer (PHOIBOS 100, SPECS GmbH). The XPS spectra were deconvoluted by using CasaXPSTM software [9].

Pd L₃-edges NEXAFS measurement

In order to avoid the air oxidation of the Mg-Pd NPs, we attempted to cover the Mg-Pd NPs with fluorine resin. The Mg-Pd NPs deposited on the PP film were inserted into the transfer vessel [10] in the high vacuum. The transfer vessel enables us to transport the Mg-Pd NPs sample to the glove box without the exposure to the air. The Mg-Pd NPs were covered with the fluorine resin under the nitrogen gas atmosphere in the glove box.

Pd L₃-edge XAFS measurements using the synchrotron radiation were carried out at BL-10 of the SR center in Ritsumeikan University [10, 11]. A Golovchenko-type double-crystal monochromator with Ge(111) was used for the monochromatization of incident X-ray. The Pd L₃-edge XAFS measurements were carried out with fluorescence X-ray yield method in flowing the dilute hydrogen gas (4 wt% H₂) for hydrogenation (100 cc/min) or He gas for dehydrogenation (500 cc/min). The acquisition time of the NEXAFS spectrum was 3.5 minutes.

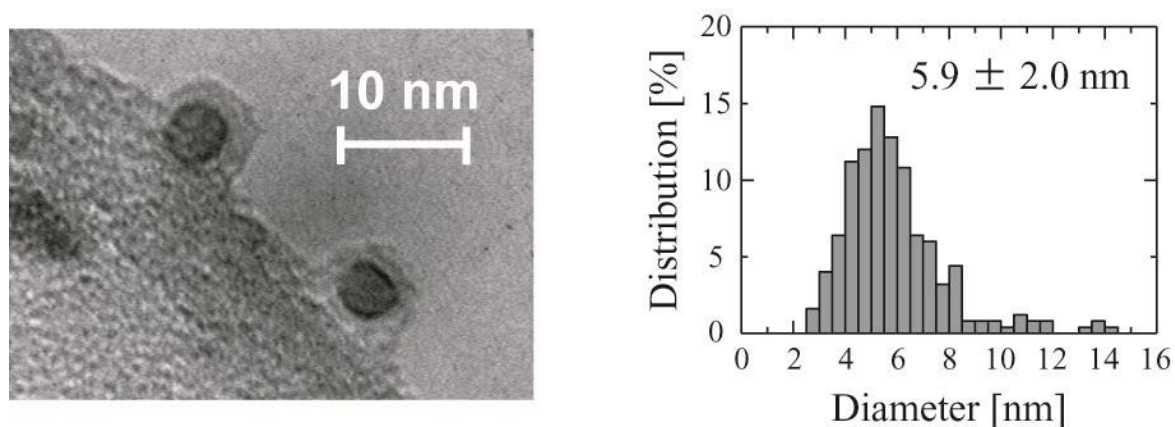


Fig. 2 The bright field image and the size distribution of the Mg-Pd NPs.

3. Results and Discussion

3.1 Surface chemical analysis by XPS

Fig. 3 shows XPS spectrum for Mg 2p and Pd 3d_{5/2} core electrons of the Mg-Pd NPs. It is noted that Pd 4p spectrum is observed around the energy region of Mg 2p spectrum when the both Mg and Pd atoms are contained on the surface of the sample. We have attempted the subtraction of the Pd 4p spectrum for the metallic Pd from the XPS spectrum around the energy range of 42 ~ 62 eV in order to derive the Mg 2p spectrum. Prior to the subtraction, the Pd 4p spectrum is normalized with respect to the peak area ratio of the Pd 3d spectra between the Mg-Pd NPs and the metallic Pd. The Mg 2p spectrum has been obtained as the residual spectrum and deconvoluted into two components. The peak locating at 50.9 eV in Fig. 3 represents Mg²⁺ associated with MgO or Mg(OH)₂. The surface of the Mg-Pd NPs has been oxidized by the residual gas such as O₂ and/or H₂O in the vacuum chamber. The peak locating at 49.5 eV represents the chemical state of the Mg-Pd alloy. We have not been able to deconvolute the Mg 2p spectrum with the peak associated with the metallic Mg (49.7 eV). The slight energy difference of the peak top positions between metallic Mg and the Mg-Pd alloy indicates that the valence electrons have been transferred from Pd atoms to Mg atoms in the Mg-Pd NPs.

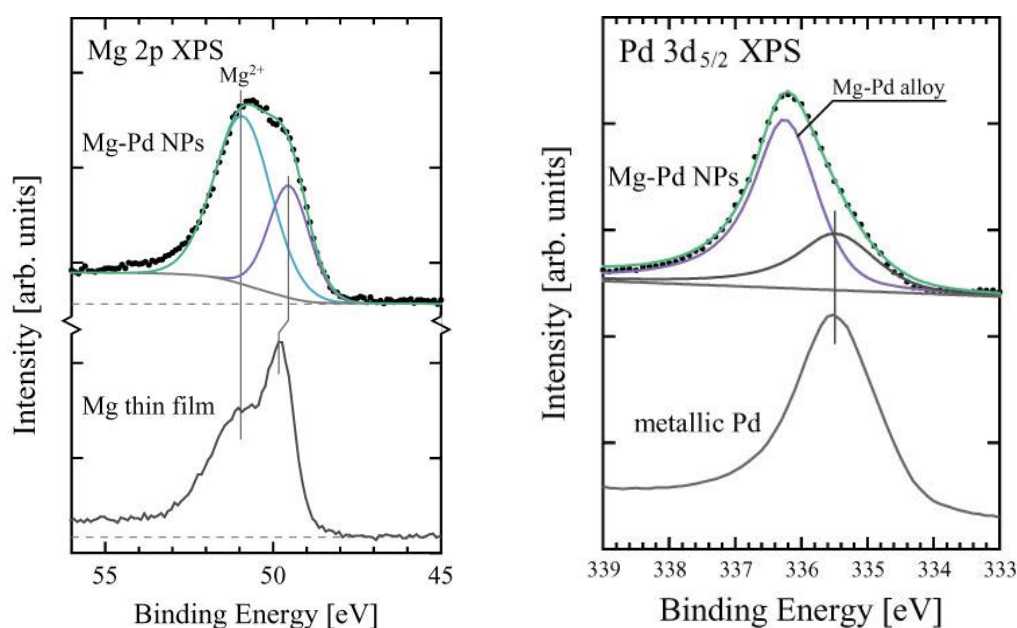


Fig. 3 The XPS spectra for the Mg 2p and Pd 3d_{5/2} core electrons of the Mg-Pd NPs. The XPS spectra of the metallic Mg and Pd are shown as the standard spectra. The Mg 2p spectrum of the Mg-Pd NPs has been obtained by subtraction of Pd 4p spectrum.

The transfer of the valence electrons is also indicated in the Pd 3d_{5/2} spectrum. The peak top of Pd 3d_{5/2} spectrum for the Mg-Pd NPs obviously shifts to higher binding energy side by about 0.8 eV. This energy shift is consistent with that of the Mg 2p spectrum. The Pd 3d_{5/2} spectrum for the Mg-Pd NPs can be deconvoluted into two components of the metallic Pd (335.5 eV) and the Mg-Pd alloy (336.3 eV). The Pd 3d_{5/2} peak associated with PdO (336.9 eV [12]) has not been observed in the spectrum of the Mg-Pd NPs.

3.2 *In-situ* NEXAFS analysis of the Mg-Pd nanoparticles

We have demonstrated the *in-situ* NEXAFS measurement system with the Pd NPs. Fig. 4 shows the Pd L₃-edge NEXAFS for the Pd NPs during hydro-/dehydrogenation. The Pd NPs have been covered with the fluorine resin prior to the NEXAFS measurement. The hydrogenation and dehydrogenation have been achieved by the exposure to the diluted hydrogen gas and He gas, respectively. The gradual change of the NEXAFS spectrum for the Pd NPs can be seen in Fig. 4 during the hydro-/dehydrogenation. The peak top shifts toward higher energy side and the peak structure (3182 eV) associated with Pd-H anti-bonding state grows gradually with the progress of the hydrogenation. The changes of the NEXAFS spectrum are reversed by the dehydrogenation. These results reveal clearly the reversibility of the hydrogenation reaction of the Pd NPs.

Fig. 5 shows the change of Pd L₃-edge NEXAFS spectrum for the Mg-Pd NPs during the hydro-/dehydrogenation. The shape of the NEXAFS spectrum for the Mg-Pd NPs before hydrogenation is quite different from that of Pd NPs. The two peak structures are seen in the NEXAFS spectrum for the Mg-Pd NPs. The first peak structure around 3176 eV is attributed to the chemical state of the metallic Pd and the second one is attributed to that of the Mg-Pd alloy. The first peak structure in the spectrum for the Mg-Pd NPs shifts slightly to the higher energy side compared with that of pure metallic Pd (3175 eV) because of the overlapping partly with the peak structures for the Mg-Pd alloy [3].

The peak structures of the NEXAFS spectra for the Mg-Pd NPs shift gradually with the progress of the hydrogenation. This peak shifts indicate the hydrogenation of the Pd or the change of the chemical state of the Mg-Pd alloy. In order to investigate the peak shift, the NEXAFS spectra in Fig. 5 have been simulated by the linear combination fitting. The fittings have been carried out with the NEXAFS spectra for the Mg-Pd NPs before hydrogenation, Pd NPs before hydrogenation and hydrogenated Pd NPs. Fig. 6 shows the simulation of the NEXAFS spectrum for the fully hydrogenated Mg-Pd NPs. The NEXAFS spectrum of the Pd NPs has been subtracted from that of the Mg-Pd NPs. The NEXAFS spectrum of the hydrogenated Pd NPs has compensated for the decline of the intensity. Fig. 7 shows the variation of the fraction of each component during the hydrogenation of Mg-Pd

NPs. The gradual decrease and increase of the fraction of the Pd NPs and hydrogenated Pd NPs are clearly shown, respectively. The fraction of the initial Mg-Pd NPs is constantly about 1, which means that the fraction of the Mg-Pd alloy has not changed during the hydrogenation.

During dehydrogenation, the two peak structures in the NEXAFS of the Mg-Pd NPs slightly shift toward the each initial energy positions. However, the complete dehydrogenation has not been observed in Fig. 5. This result indicates that the Pd phase has not been dehydrogenated under the He gas atmosphere. The Pd phase in the Mg-Pd NPs has been hydrogenated under the even if diluted hydrogen gas atmosphere. Fig. 5 represents that the hydrogenated Pd phase has remained under the He gas. The remained hydrogenated Pd in the Mg-Pd NPs suggests that a part of Pd phases is surrounded by the MgH₂ layers during the hydrogenation. Hydrogen atoms can be easily absorbed and desorbed via the uncovered Pd surface at the room temperature [2]. However, the covered Pd surface by the envelope with the low hydrogen diffusion property such as MgH₂ can not release the hydrogen due to the inhibition of the hydrogen diffusion thorough the envelope. The MgH₂ layer might be migrated toward the surface of the Mg-Pd NPs during the hydrogenation by the Kirkendall effect [13]. The affinity of interaction between Mg and hydrogen can cause the diffusion of Mg atoms. The mixture of Mg and Pd phases is favorable for the hydrogenation of Mg. However, it can not play a role in the dehydrogenation of the MgH₂.

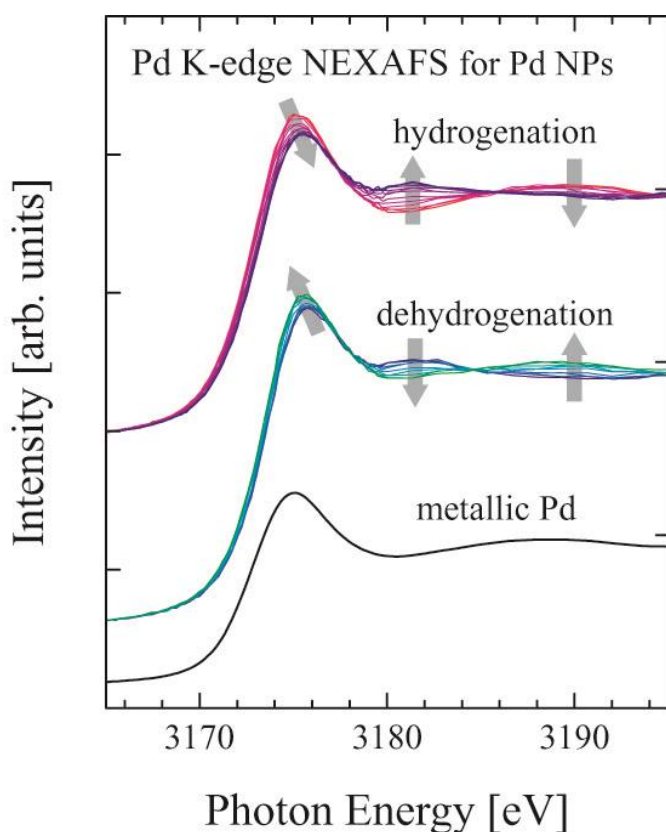


Fig. 4 The change of the Pd L₃-edge NEXAFS for the Pd NPs during the hydro- /dehydrogenation. The spectrum of the metallic Pd is shown as the standard.

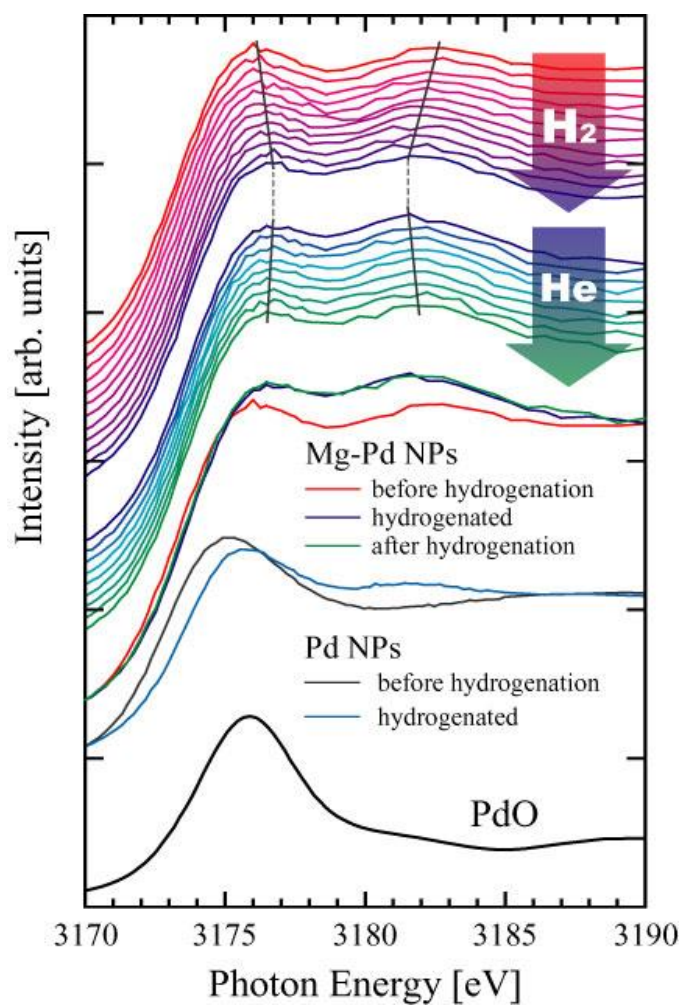


Fig. 5 The change of the Pd L₃-edge NEXAFS for the Mg-Pd NPs during the hydro- /dehydrogenation. The spectra of the Mg-Pd NPs and Pd NPs before hydrogenation or hydrogenated are also shown. The spectrum of the PdO is shown as the standard.

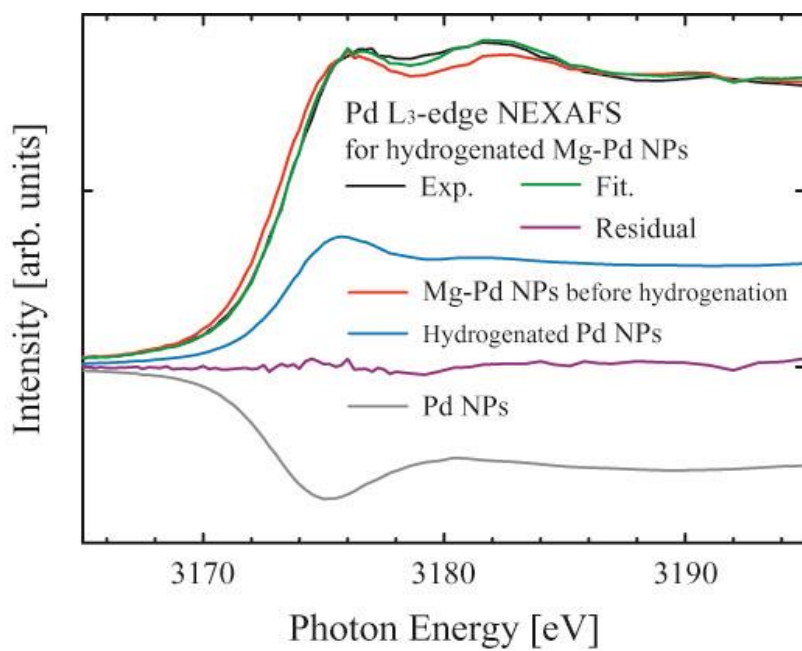


Fig. 6 The simulation of the Pd L₃-edge NEXAFS of the Mg-Pd NPs after hydrogenation by the linear combination fitting.

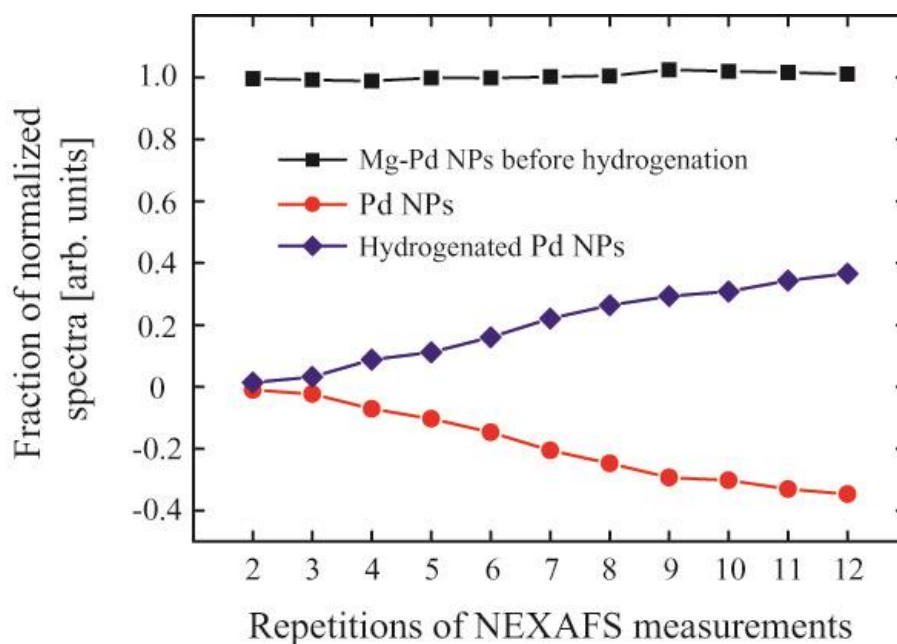


Fig. 7 The fraction of the normalized spectra for the components in the simulated spectra.

4. Conclusions

The Mg-Pd NPs have been fabricated by the gas evaporation method with He gas and investigated by XPS and *in-situ* Pd L₃-edge NEXAFS measurements. Both XPS and NEXAFS analyses indicate that the Mg-Pd NPs are composed of the metallic Pd and the Mg-Pd alloy phases. The valence electron of the Pd is transferred to the Mg in the alloy phase. The hydrogenation of the Pd phase has been seen clearly by the *in-situ* NEXAFS measurements. On the other hand, the subsequent dehydrogenation of the Pd phase has not been observed under the He gas atmosphere, although the dehydrogenation of the pure Pd NPs has been confirmed at the same condition. The inhibition of the dehydrogenation implies that the Pd phase on the Mg-Pd NPs has been covered with the MgH₂ layer. The both hydrogen dissociation and recombination reactions occur on the Pd surfaces. The covering MgH₂ layer has prohibited these reactions on the surface of the Mg-Pd NPs.

Acknowledgement

The authors are grateful for the financial support of a Grant-in-Aid for Scientific Research (B) (No. 24360332) from the Japan Society for the Promotion of Science (JSPS) and JSPS Research Fellowship for Young Scientists (No. 236237). This work was performed under the approval of Ritsumeikan University SR center Program Advisory Committee (Nos. R1316 and R1345).

References

- (1) I.P. Jain, C. Lal, A. Jaini, *Int. J. Hydro. Ener.*, **2010**, 35, 5133.
- (2) K. Yoshimura, Y. Yamada, M. Okada, *Surf. Sci.*, **2004**, 566-568, 751.
- (3) S. Ogawa, T. Mizutani, M. Ogawa, C. Yogi, T. Ohta, T. Yoshida, S. Yagi, *Confer. Proc. NANOCON 2012*, **2012**, ISBN 978-80-87294-32-1, 274.
- (4) V. Tsionsky and E. Gileadi, *Langmuir*, **1994**, 10, 2830.
- (5) I. Kulchytsky, M. G. Kocanda and T. Xu, *Appl. Phys. Lett.*, **2007**, 91, 113507.
- (6) A. Baldi, M. Gonzalez-Silveira, V. Palmisano, B. Dam, R. Griessen, *Phys. Rev. Lett.*, **2009**, 102, 226102.
- (7) C.-J. Chung, S.-C. Lee, J. R. Groves, E. N. Brower, R. Sinclair, B. M. Clemens, *Phys. Rev. Lett.*, **2012**, 108, 106102.
- (8) S. Ogawa, S. Murakami, K. Shirai, K. Nakanishi, C. Tsukada, T. Ohta and S. Yagi, *e-J. Surf. Sci. Nanotech.*, **2011**, 9, 315.
- (9) N. Fairley, CasaXPS Version 2.3.13 Dev22: Software package for data processing.
<http://www.casaxps.com>
- (10) K. Nakanishi, S. Yagi, and T. Ohta, *IEEJ Trans. EIS*, **2010**, 130, 1762.
- (11) K. Nakanishi, S. Yagi, T. Ohta, *AIP Conf. Proc.*, **2010**, 1234, 931.
- (12) S. Murakami, S. Ogawa, K. Shirai, C. Tsukada, S. Yagi, K. Nakanishi, T. Ohta, *e-J. Surf. Sci. Nanotech.*, **2011**, 9, 438.
- (13) G. Krishnan, B. J. Kooi, G. Palasantzas, Y. Pivak, and B. Dam, *J. Appl. Phys.*, **2010**, 107, 053504.